

Pre-main sequence variable stars in young open cluster NGC 1893

Sneh Lata^{1*}, A. K. Pandey¹, W. P. Chen², G. Maheswar¹ and Neelam Chauhan²

¹*Aryabhata Research Institute of Observational Sciences, Manora Peak, Nainital 263129, Uttarakhand, India*

²*Institute of Astronomy, National Central University, Chung-Li 32054, Taiwan*

Accepted ———. Received ———;

ABSTRACT

We present results of multi-epoch (fourteen nights during 2007-2010) V -band photometry of the cluster NGC 1893 region to identify photometric variable stars in the cluster. The study identified a total of 53 stars showing photometric variability. The members associated with the region are identified on the basis of spectral energy distribution, $J - H/H - K$ two colour diagram and $V/V - I$ colour-magnitude diagram. The ages and masses of the majority of pre-main-sequence sources are found to be $\lesssim 5$ Myr and in the range $0.5 \lesssim M/M_{\odot} \lesssim 4$, respectively. These pre-main-sequence sources hence could be T Tauri stars. We also determined the physical parameters like disk mass and accretion rate from the spectral energy distribution of these T Tauri stars. The periods of majority of the T Tauri stars range from 0.1 to 20 day. The brightness of Classical T Tauri stars is found to vary with larger amplitude in comparison to Weak line T Tauri stars. It is found that the amplitude decreases with increase in mass, which could be due to the dispersal of disks of massive stars.

Key words: Open cluster: NGC 1893 – colour-magnitude diagram: Variables-pre-main sequence stars

1 INTRODUCTION

It is now well established that circumstellar disks are an integral part of star formation and are potential sites for planet formation (e.g. Hillenbrand 2002). Young star clusters have significant number of pre-main-sequence (PMS) stars with circumstellar disk and are unique laboratories to study the evolution of disks of PMS stars. PMS objects are generally classified into T Tauri stars (TTSS) and Herbig Ae/Be stars. The TTSSs have masses $\lesssim 3 M_{\odot}$ which are contracting towards the main-sequence (MS), whereas Herbig Ae/Be stars have masses in the range of ~ 3 -10 M_{\odot} . These stars are contracting towards MS or just reached the MS. On the basis of the strength of the $H\alpha$ emissions, the TTSSs are further classified as Weak line TTSSs (WTTSSs; equivalent width (EW) $\leq 10 \text{ \AA}$) or Classical TTSSs (CTTSSs; $\text{EW} > 10 \text{ \AA}$). Both WTTSSs and CTTSSs show variation in their brightness. These variations are found to occur at all wavelengths, from X-ray to infrared. Variability time scale of TTSSs ranges from few minutes to years (Appenzeller & Mundt 1989). The photometric variations are believed to originate from several mechanisms like rotation of a star with an asymmetrical distribution of cool spots, variable hot spots or obscuration by circumstellar dust (see Herbst et al. 1994 and reference therein). The Her-

big Ae/Be stars also show variability as they move across the instability region in the Hertzsprung-Russell (HR) diagram on their way to the MS. Several systematic studies of TTSSs have been carried out which revealed different type of variabilities (Herbst et al. 1994). It is now well known that some of them show periodic variability (e.g., Hillenbrand 2002; Schaefer 1983; Bouvier et al. 1993; Bouvier 1994; Percy et al. 2006, 2010).

NGC 1893 ($l = 173^{\circ}.58$ and $b = -01^{\circ}.68$) is a young cluster (age ~ 4 Myr) having a significant population of PMS sources (Sharma et al. 2007). NGC 1893, located at a distance of 3.25 kpc (Sharma et al. 2007) contains a number of early type stars, a bright diffuse nebulosity and two penant nebulae, Sim 129 and Sim 130 (Gaze & Shajn 1995). The region also contains at least five O-type stars (Hiltner 1966). Efforts have been made by a number of authors to identify low mass PMS stars towards the cluster NGC 1893. On the basis of optical and near infra-red (NIR) photometry, Vallenari et al. (1999) suggested that there could be a significant number of PMS stars in the cluster region with a large spread in their ages. Using the $uvby\beta$ CCD photometry of the region Marco et al. (2001) identified ~ 50 likely members (spectral type B9-A0) in the cluster. Marco et al. (2001) also suggested the existence of a significant PMS population in the cluster. In a later study, based on low resolution spectroscopy, Marco & Negueruela (2002) con-

* E-mail: sneh@aries.res.in

Table 1. Log of the observations. N and Exp. represent number of frames obtained and exposure time respectively.

S. No.	Date of observations	Object	V (N×Exp.)	I (N×Exp.)
1	05 Dec 2007	NGC 1893	3×40s	-
2	08 Dec 2007	NGC 1893	3×50s	-
3	07 Jan 2008	NGC 1893	2×40s	-
4	10 Jan 2008	NGC 1893	3×50s	-
5	12 Jan 2008	NGC 1893	80×50s	-
6	14 Jan 2008	NGC 1893	70×40s	-
7	29 Oct 2008	NGC 1893	97×50s	-
8	21 Nov 2008	NGC 1893	137×50s	2×50s
9	27 Jan 2009	NGC 1893	5×50s	-
10	28 Jan 2009	NGC 1893	5×50s	-
11	19 Feb 2009	NGC 1893	5×50s	-
12	20 Feb 2009	NGC 1893	3×50s	5×50s
13	20 Feb 2009	SA 98	5×90s	5×60s
14	31 Oct 2010	NGC 1893	3×50s	-

firmed the PMS nature of a number of sources. Maheswar et al. (2007) and Negueruela et al. (2007) identified additional numbers of emission-line and NIR excess sources. A significant number of these sources are found concentrated towards regions near Sim 129 and Sim 130. Maheswar et al. (2007) and Sharma et al. (2007) gave evidence for triggered star formation in the region. Recently on the basis of optical, NIR, mid-infra red (MIR) and X-ray data Prisinzano et al. (2011) have identified 1034 and 442 Class II and Class III sources, respectively, in the region.

In this study, we present results of our multi-epoch photometric monitoring of the region containing NGC 1893. The observations in the V band have been carried out on 14 nights from December 2007 to October 2010 in order to identify and characterize the variable stars in the NGC 1893 region. In Section 2 we discuss the observations, data reduction procedure and the spatial distribution of variables. Section 3 deals with the membership based on the spectral energy distribution, $V/V - I$ colour-magnitude diagram (CMD) and $J - H/H - K$ two colour diagram (TCD). Section 4, 5 and 6 describe period determination, physical state of variables and characteristics of variables. Finally, we conclude our paper with a summary of the main results obtained in the current study in Section 7.

2 OBSERVATIONS AND DATA REDUCTION

The photometric monitoring of the NGC 1893 region was carried out in the V -band on 14 nights and in the I -band on two nights from 2007 December 05 to 2010 October 31 using a 2048×2048 CCD camera attached to the 104 cm Sampurnanand ARIES telescope. The field of view is $\sim 13' \times 13'$ and the scale is $\sim 0.76''/\text{pixel}$ in 2×2 pixel binning mode. The central position on the sky was close to RA (2000) = $05^h 22^m 42^s$ and Dec (2000) = $+33^\circ 25' 00''$ for all the frames. On each night, at least two frames of target field were obtained in the V -band to cover long period variables. Fig. 1, taken from Digital Sky Survey (DSS), displays the observed region of NGC 1893. The observations of NGC 1893 consist of a total of 421 CCD images in the V -band. The typical seeing (estimated from the FWHM of the point like stars)

of the images was found to be $1.5'' - 2''$. Bias and twilight flats were also taken along with the target field. The log of the observations is given in Table 1.

2.1 Photometry

The preprocessing of the CCD images was performed by using the IRAF¹, which includes bias subtraction, flat field correction and removal of cosmic rays. The instrumental magnitude of the stars were obtained using the DAOPHOT package (Stetson 1987). Both aperture and PSF photometry were carried out to get the magnitude of the stars. The PSF photometry yields better results for crowded regions. We have used the DAOMATCH (Stetson 1992) routine of DAOPHOT to find the translation, rotation and scaling solutions between different photometry files, whereas DAOMASTER (Stetson 1992) matches the point sources. To remove frame-to-frame flux variation due to airmass and exposure time, we used DAOMASTER programme to get the corrected magnitude. This task makes the mean flux level of each frame equal to the reference frame by an additive constant. The first target frame taken on 21 November 2008 has been considered as the the reference frame. Present observations have 421 frames and each frame corresponds to one photometry file. The DAOMASTER cross identified 1186 stars in different photometry files and listed their corrected magnitudes in a .cor file. We have considered only those stars for further study which have at least 100 observations. The data file (.cor) generated by DAOMASTER programme was used to identify variable candidates in the next section.

The standardization of the cluster fields was carried out by observing the standard field SA 98 (Landolt 1992). The standardization procedure is outlined below. First, we have standardised the cluster region using the observations of the region and standard field SA 98 taken on 20 Feb 2009. The instrumental magnitudes were transformed to the standard Johnson V and Cousins I system using the procedure outlined by Stetson (1992). The equations used for photometric calibration are given below:

$$v = V + a_1 - b_1 \times (V - I) + 0.26 \times Q$$

$$i = I + a_2 - b_2 \times (V - I) + 0.16 \times Q$$

where v and i are the instrumental magnitudes and Q is the airmass. The values of a_1 , a_2 , b_1 , and b_2 are 5.009 ± 0.007 , 5.357 ± 0.012 , 0.0496 ± 0.006 , and 0.0575 ± 0.010 respectively. Stars spread all over the cluster region were selected as secondary standards. The secondary standards were used to standardise the reference frame.

2.2 Comparison with Previous Photometry

We have compared present CCD photometric data with the latest CCD photometry given by Sharma et al. (2007), and its was found that 957 stars are common between these two data sets. Fig. 2 shows the difference Δ (present data

¹ IRAF is distributed by the National Optical Astronomy Observatory, which is operated by the Association of Universities for Research in Astronomy (AURA) under cooperative agreement with the National Science Foundation.

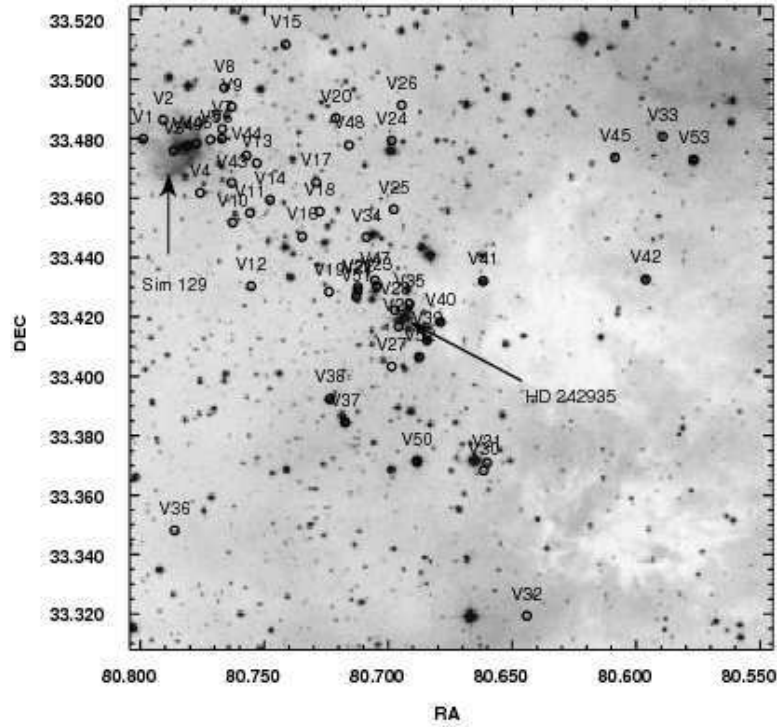


Figure 1. The observed region of NGC 1893 (image taken from the DSS-R). The circles show the location of variables identified in the present work.

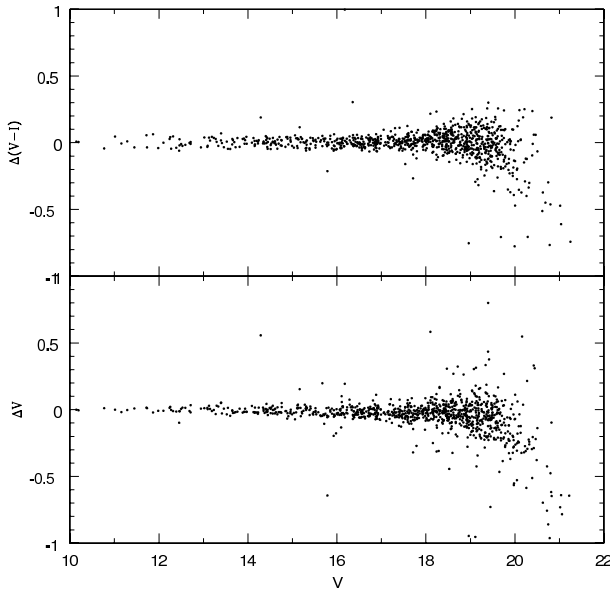


Figure 2. Comparison of the present photometry and photometry given by Sharma et al. (2007). The Δ represents present minus previous photometry.

-literature data) as a function of V magnitude. The comparison indicates that the present photometric data are in very good agreement with the CCD photometry by Sharma et al. (2007). The present V magnitudes and $(V - I)$ colours are also in fair agreement with those given by Sharma et al. (2007).

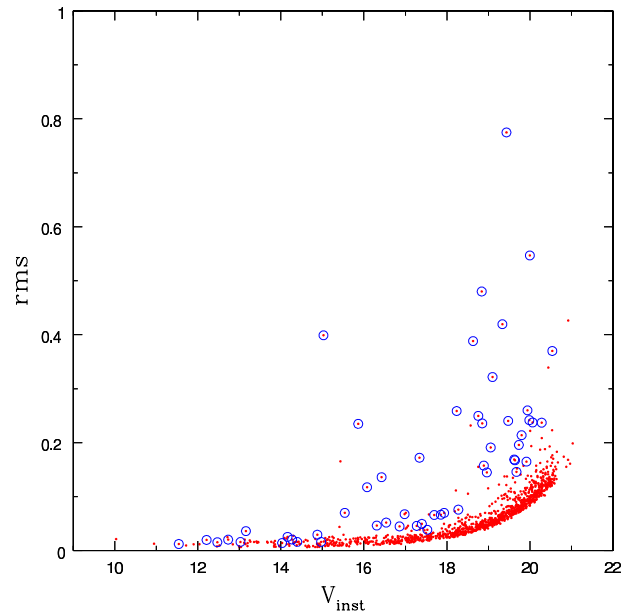


Figure 3. The rms for each star as a function of brightness. The open circles represent candidate variables identified in the present work.

2.3 Identification of Variables

The mean value of the magnitude and rms of data for each star were estimated using all the observations. The rms dispersion as a function of instrumental magnitude is shown in Fig. 3, which indicates that the majority of the stars fol-

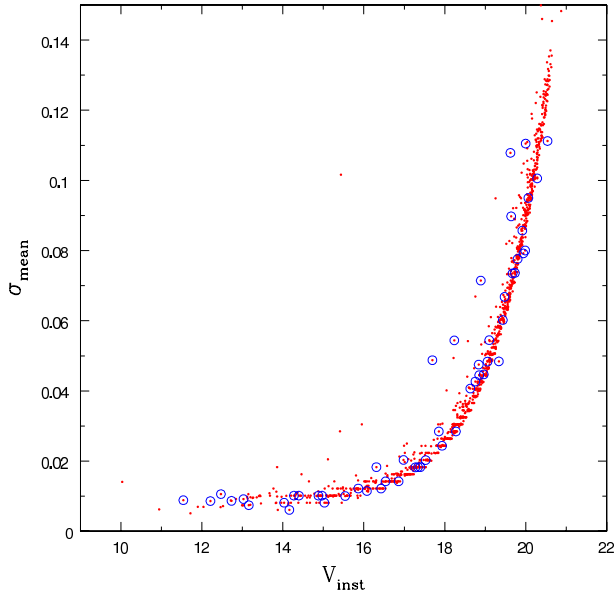


Figure 4. Mean photometric errors as a function of brightness. Open circles represent the same as in Fig. 3.

low an expected trend i.e., the S/N ratio decreases as stars become fainter. However, a few stars do not follow the normal trend and exhibit relatively large scatter. These could be either due to the large photometric errors or due to the variable nature of the stars. We considered a star as variable if its rms is greater than 3 times of the mean rms of that magnitude bin. Around 60 candidate variables were thus identified on the basis of the above mentioned criterion. A careful inspection of light curves and the location of the sources on the CCD frames rejected a few stars as they were lying near the edge of the CCD. Finally, the present sample of variable stars has 53 variable candidates. The identification number, coordinates and photometric data for these variable stars are given in Table 2. The mean value of photometric error of the data was estimated using the observations of each star. The mean error (σ_{mean}) as a function of instrumental magnitude is shown in Fig. 4. The mean error is found to be ~ 0.01 mag at magnitude ≤ 16 mag, whereas its value increases to ~ 0.1 mag at ~ 20 mag. The light curves of a few variables are shown in Fig. 5. Table 2 also lists NIR and MIR data taken from Prisinzano et al. (2011). The $[3.4 \mu\text{m}]$, $[4.6 \mu\text{m}]$, $[12 \mu\text{m}]$, and $[22 \mu\text{m}]$ data have been taken from the WISE database (<http://irsa.ipac.caltech.edu/>).

In Fig. 1, we present the spatial distribution on the DSS image of the variable stars detected in the present study. The distribution shows a rather aligned distribution from the ionising source of the region (HD 242935) to the nebula Sim129. The spatial distribution of variable stars is found to be similar to that of $H\alpha$ emission line stars and NIR excess sources (Marco & Negueruela 2002; Maheswar et al. 2007; Sharma et al. 2007), which suggests that these variable stars should be a part of young stellar population and associated with the NGC 1893 star forming region.

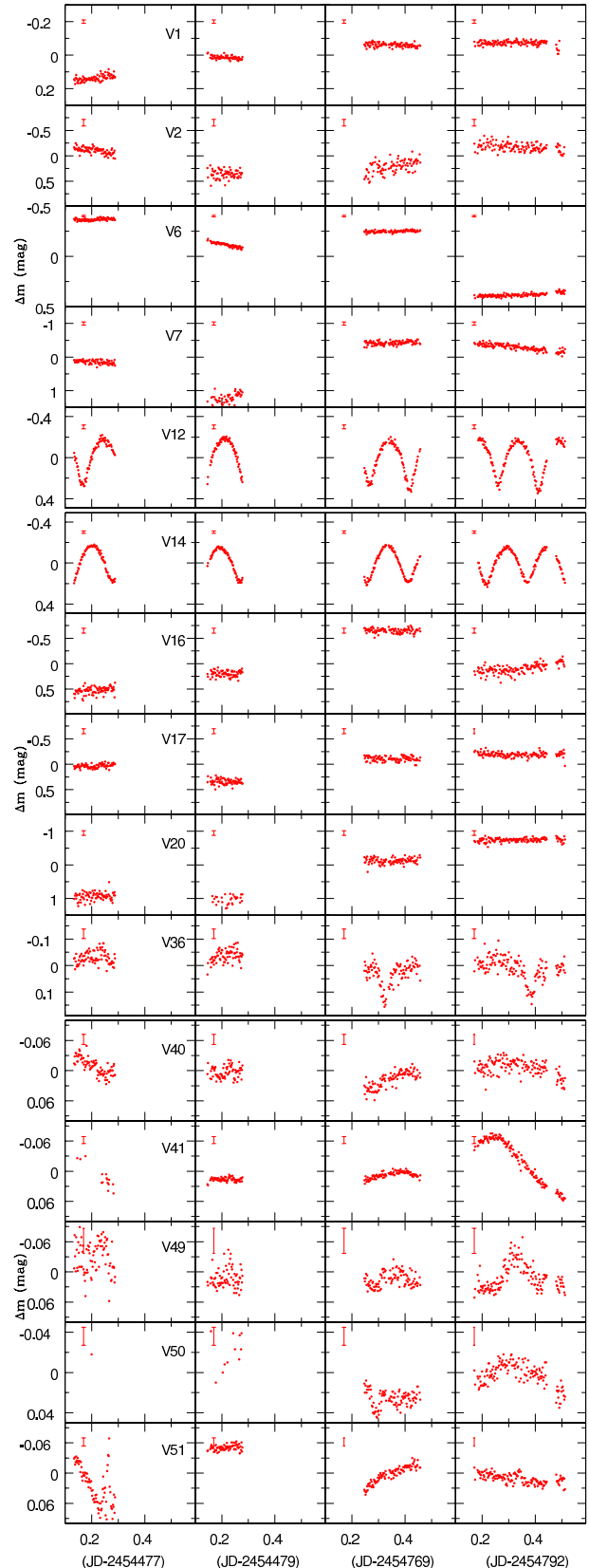


Figure 5. The light curves of few variable stars identified in the present work. The typical errors of observations are also shown. The Δm represents the differential magnitude in the sense that variable minus comparison star.

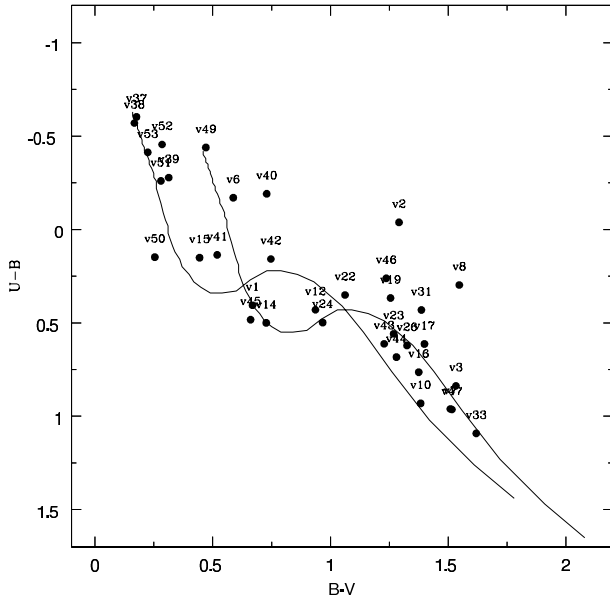


Figure 6. $U - B/B - V$ two colour diagram. The UBV data have been taken from Sharma et al. (2007). The solid line represents the ZAMS by Girardi et al. (2002) shifted along the reddening vector of 0.72 for $E(B - V)_{min} = 0.4$ mag and $E(B - V)_{max} = 0.7$ mag.

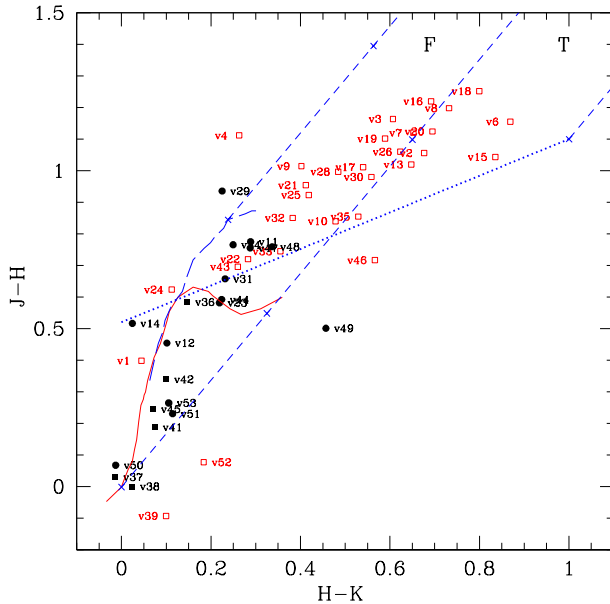


Figure 7. $(J - H)/(H - K)$ TCD for stars lying in the field of 13×13 arcmin of NGC 1893. JHK data have been taken from Prisinzano et al. (2011). The sequences for dwarfs (solid) and giants (long dashed) are from Bessell & Brett (1988). The dotted line represents the locus of TTSs (Meyer et al. 1997). The small dashed lines represent the reddening vectors (Cohen et al. 1981). The crosses on the reddening vectors represent an increment of visual extinction of $A_V = 5$ mag.

The open squares and filled circles represent the Class II and Class III sources identified by Prisinzano et al. (2011). The filled squares represent those stars which were not cross identified in Prisinzano catalogue.

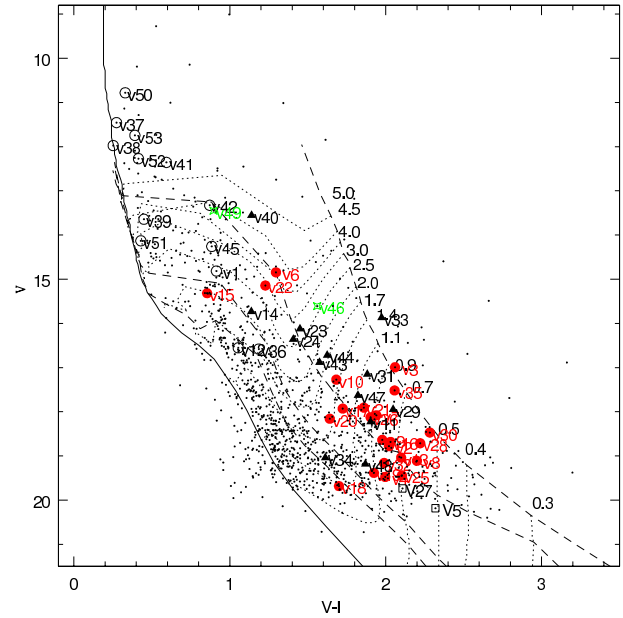


Figure 8. $V/V - I$ colour-magnitude diagram for the cluster NGC 1893. The small dots represent all the sources in the observed field. The filled circles and triangles represent CTTSs and WTTSs Table 3. The open circles represent non-PMS stars. The probable YSOs (V5, V27, V36 and V42) are shown with open squares. Star symbols represent Herbig Ae/Be stars (V46 and V49). The ZAMS by Girardi et al. (2002) and PMS isochrones for 0.1, 1, 5, 10 Myrs by Siess et al. (2000) are shown. The dotted curves show PMS evolutionary tracks of stars of different masses. The isochrones and evolutionary tracks are corrected for the cluster distance and $E(V - I) = 0.50$ mag.

the α index. Keeping the error in mind these could be either Class II or Class III sources.

3.3 $U - B/B - V$ and $J - H/H - K$ two colour Diagram

The $U - B/B - V$ TCD for variable candidates is plotted in Fig. 6. The UBV data for variable candidates have been taken from Sharma et al. (2007). The distribution of stars in the $U - B/B - V$ TCD indicates a variable reddening in the cluster region with $E(B - V)$ from ~ 0.4 to 0.7 mag. It is not possible to estimate the $E(B - V)$ for the YSOs since the U and B band fluxes may be affected by excess due to accretion which could be an important origin for the scattering of the sources in $U - B/B - V$ TCD.

The NIR TCD diagram is also useful to identify the CTTS and WTTS. Fig. 7 shows the near $J - H/H - K$ TCD. The JHK data catalogued by Prisinzano et al. (2011) are in MKO system which were converted to 2MASS system using relations given on the website². After that JHK data from both the catalogues (Prisinzano catalogue and 2MASS catalogue) were transformed to CIT system using the relations given on the above mentioned website. The solid and long dashed lines in Fig. 7 represents unreddened MS and giant loci (Bessell & Brett 1988) respectively. The dotted line indicates the intrinsic locus of CTTSs (Meyer et al. 1997).

² <http://www.astro.caltech.edu/jmc/2mass/v3/transformations/>

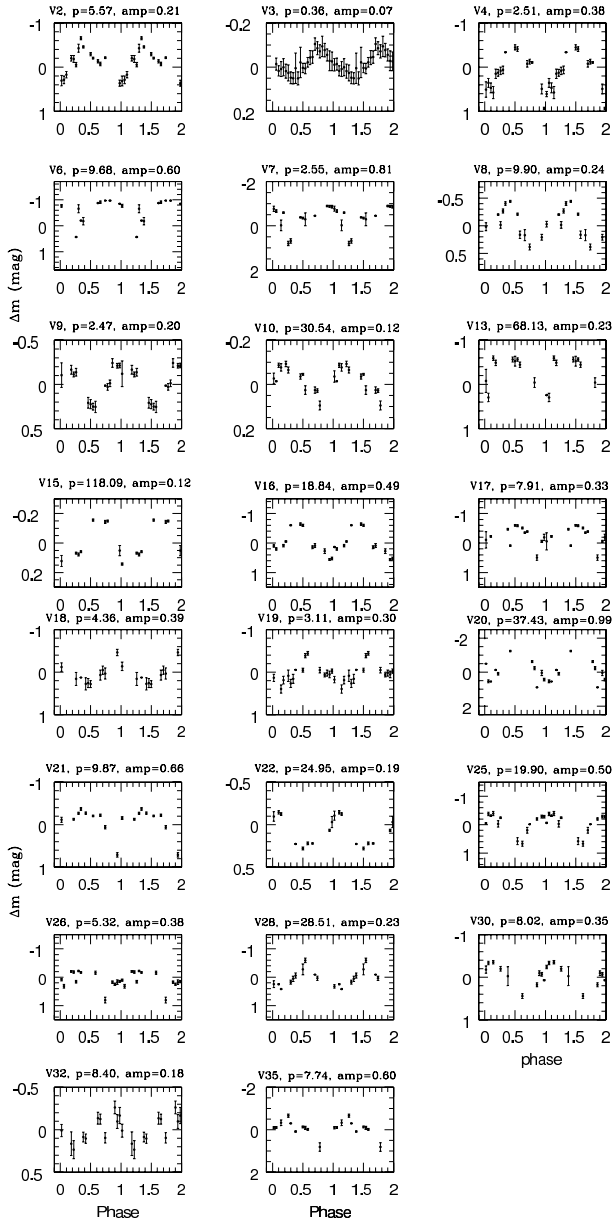


Figure 9. The phased light curves of probable CTTS candidate variables identified in NGC 1893. The Period is in days and amp is in mag.

The parallel dashed lines are the reddening vectors drawn from the tip (spectral type M4) of the giant branch (‘left reddening line’), from the base (spectral type A0) of the main-sequence branch (‘middle reddening line’) and from the tip of the intrinsic CTTS line (‘right reddening line’). The extinction ratios $A_J/A_V = 0.265$, $A_H/A_V = 0.155$ and $A_K/A_V = 0.090$ have been adopted from Cohen et al. (1981). The sources lying in ‘F’ region could be either field stars (MS stars, giants) or Class III and Class II sources with small NIR excesses. The sources lying in the ‘T’ region are considered to be mostly CTTSs (Class II objects). Majority of the the Class II sources are distributed in the ‘T’ or near the middle reddening vector in the ‘F’ region. The locations of V24 and V33 in NIR TCD also indicate that these sources should be diskless class III instead of Class II as suggested

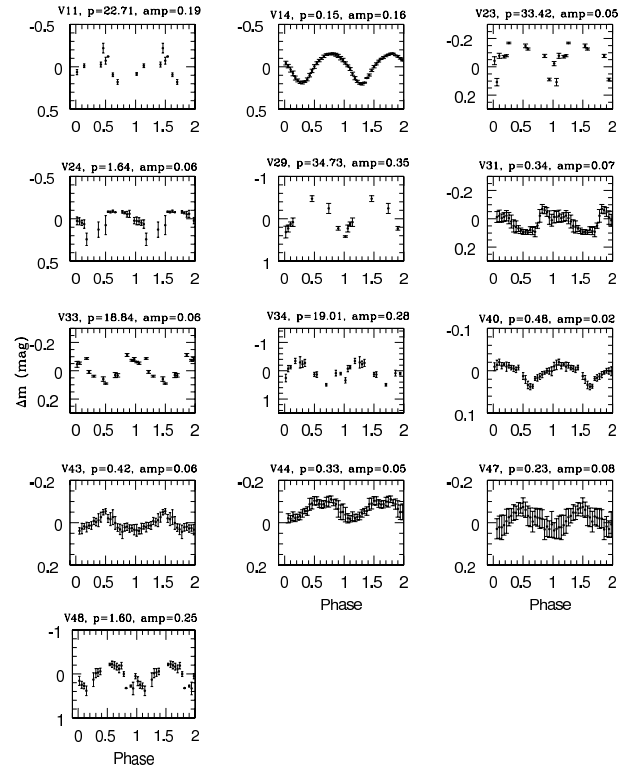


Figure 10. The phased light curves of probable WTTS candidate variables identified in NGC 1893. The Period is in days and amp is in mag.

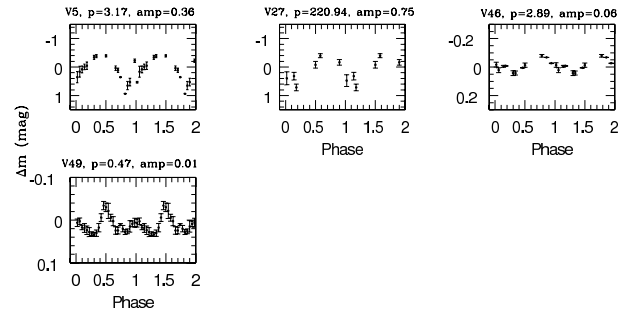


Figure 11. The phased light curves of probable YSOs. The Period is in days and amp is in mag.

by Prisinzano et al. (2011) on the basis of MIR TCD. The star V1 is classified as Class I/II source by Prisinzano et al. (2011), whereas its location in NIR TCD as well as in $U - B/B - V$ TCD manifests that it should be late B-type MS star. The location of V43 in the NIR TCD suggests that it could be a WTTS. The location of V12 in the NIR TCD and $U - B/B - V$ TCD suggests that it could be an MS star. Star V39 was classified as Class II by Prisinzano et al. (2011), however its location in NIR TCD and $U - B/B - V$ TCD indicates that it could be an MS or Herbig Be star. The location of stars numbered V36, V37, V38, V41, V42, V45 in the NIR TCD as well as in $U - B/B - V$ TCD suggests that these stars could be MS stars. The stars V50 and V51 are found to be diskless/class III source on the basis of Prisinzano et al. (2011) classification as well as on the basis of α index. The location of these variables in the NIR TCD

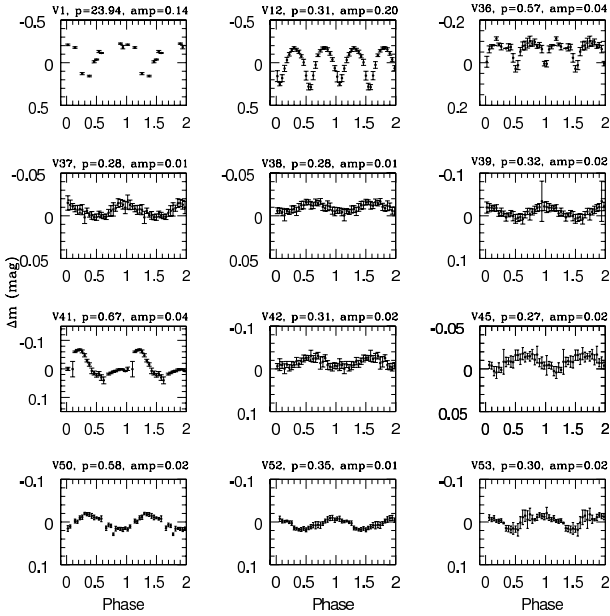


Figure 12. The phased light curves of non-PMS stars. The Period is in days and amp is in mag.

(Fig. 7) and in $U - B/B - V$ TCD reveals that these could be reddened O/ B-type stars. The location of V52 and V53 in NIR TCD and $U - B/B - V$ TCD as well as α index indicates that these stars could be MS stars. Prisinzano et al. (2011) on the basis of MIR TCD identified V52 and V53 as class II and diskless/class III source respectively.

The classification of variables adopted in the present study on the basis of MIR data, SEDs, NIR TCD and $U - B/B - V$ TCD is given in the last column of Table 3.

3.4 $V/V - I$ colour-magnitude diagram

Fig. 8 shows the $V/V - I$ CMD for all the stars identified (small dots) in the cluster region NGC 1893. The filled circles and triangles represent probable CTTs and WTTs respectively, whereas open circles represent non-PMS variable stars which are classified in section 3.3 on the basis $J - H/H - K$ and $U - B/B - V$ TCDs. The variables V5 and V27 do not have JHK data however they lie in the PMS region of the CMD. These are represented by open squares and are considered as YSOs. Two stars V46 and V49 which could be Herbig Ae/Be stars are represented by star symbols in Fig. 8. In Fig. 8 we have also plotted theoretical isochrone for 4 Myr for $Z=0.02$ (continuous line) by Girardi et al. (2002) and PMS isochrones for various ages and evolutionary tracks for various masses by Siess et al. (2000). All the isochrones and evolutionary tracks are corrected for the distance (3.25 kpc) and minimum reddening $E(V - I)=0.50$ mag. The minimum value of $E(V - I)$ has been estimated using the relation $E(V - I)/E(B - V) = 1.25$ and $E(B - V) = 0.40$ mag.

The ages of YSOs have been derived by comparing their locations with the PMS isochrones, whereas masses of PMS variable stars were determined with the help of PMS evolutionary tracks. The ages of majority of the YSOs are in the range from 0.1 Myr to 5 Myrs which are comparable with the lifetime of TTSs and the masses of these sources

Table 4. The mass, age, amp, and period of the 52 variables.

ID	Mass M_{\odot}	Age Myrs	Amp. mag	Period day
V1	-	-	0.14	23.94
V2	0.74 ± 0.05	0.72 ± 0.03	0.21	5.57
V3	0.98 ± 0.01	0.10 ± 0.01	0.07	0.36
V4	0.79 ± 0.09	1.54 ± 0.44	0.38	2.51
V5	0.51 ± 0.06	1.12 ± 0.25	0.36	3.17
V6	3.94 ± 0.15	0.64 ± 0.14	0.60	9.68
V7	0.86 ± 0.05	0.45 ± 0.03	0.81	2.55
V8	0.58 ± 0.05	0.61 ± 0.09	0.24	9.90
V9	0.80 ± 0.05	0.68 ± 0.04	0.20	2.47
V10	1.46 ± 0.11	0.53 ± 0.09	0.12	30.54
V11	0.90 ± 0.06	0.55 ± 0.07	0.19	22.71
V12	-	-	0.20	0.31
V13	0.66 ± 0.05	0.75 ± 0.12	0.23	68.13
V14	2.48 ± 0.09	3.12 ± 0.38	0.16	0.15
V15	2.33 ± 0.06	4.36 ± 0.55	0.12	118.09
V16	0.73 ± 0.04	0.67 ± 0.02	0.49	18.84
V17	1.24 ± 0.08	0.79 ± 0.12	0.33	7.91
V18	1.14 ± 0.03	8.43 ± 2.76	0.39	4.36
V19	0.88 ± 0.10	1.84 ± 0.55	0.30	3.11
V20	1.42 ± 0.09	1.49 ± 0.28	0.99	37.43
V21	0.99 ± 0.06	0.49 ± 0.05	0.66	9.87
V22	3.35 ± 0.19	1.22 ± 0.31	0.19	24.95
V23	2.85 ± 0.15	0.62 ± 0.11	0.05	33.42
V24	2.75 ± 0.08	0.93 ± 0.21	0.06	1.64
V25	0.66 ± 0.05	1.02 ± 0.21	0.50	19.90
V26	0.91 ± 0.05	0.51 ± 0.06	0.38	5.32
V27	0.67 ± 0.07	1.40 ± 0.38	0.75	220.94
V28	0.60 ± 0.07	0.42 ± 0.24	0.23	28.51
V29	0.77 ± 0.06	0.30 ± 0.12	0.35	34.73
V30	0.57 ± 0.01	0.11 ± 0.03	0.35	8.02
V31	1.06 ± 0.06	0.28 ± 0.02	0.07	0.34
V32	0.78 ± 0.06	1.07 ± 0.13	0.18	8.40
V33	1.60 ± 0.01	0.10 ± 0.01	0.06	18.84
V34	1.33 ± 0.03	5.27 ± 1.35	0.28	19.01
V35	0.81 ± 0.02	0.16 ± 0.07	0.60	7.74
V36	-	-	0.04	0.57
V37	-	-	0.01	0.28
V38	-	-	0.01	0.28
V39	-	-	0.02	0.32
V40	4.83 ± 0.06	0.45 ± 0.02	0.02	0.48
V41	-	-	0.04	0.67
V42	-	-	0.02	0.31
V43	1.90 ± 0.13	0.60 ± 0.10	0.06	0.42
V44	1.78 ± 0.12	0.42 ± 0.06	0.05	0.33
V45	-	-	0.02	0.27
V46	2.74 ± 0.17	0.27 ± 0.03	0.06	2.89
V47	1.09 ± 0.08	0.44 ± 0.05	0.08	0.23
V48	0.95 ± 0.09	1.73 ± 0.46	0.25	1.60
V49	4.61 ± 0.04	0.58 ± 0.03	0.01	0.47
V50	-	-	0.02	0.58
V52	-	-	0.01	0.35
V53	-	-	0.02	0.30

range from ~ 0.5 to $\sim 4 M_{\odot}$. The associated errors in determination of age and mass can be of two kinds; random errors in observations and systematic errors due to the use of different theoretical evolutionary tracks. We have estimated the effect of random errors in determination of age and mass by propagating the random errors to the observed estimations of $V, V - I$ and $E(V - I)$ by assuming normal error distribution and using the Monte Carlo simulations (see e.g., Chauhan et al. 2009). Since we have used model by Siess et al. (2000) only for all the PMS stars, present age and mass estimations are not affected by the systematic errors. The presence of binaries may be another source of error. The presence of binary will brighten a star, consequently the CMD will yield a lower age estimate. In the case of equal mass binary, we expect an error of ~ 50 to 60% in age estimation of the PMS stars. However, it is difficult to estimate the influence of binaries on mean age estimation as the fraction of binaries is not known. The estimated ages and masses alongwith their errors are given in Table 4.

4 PERIOD DETERMINATION

We used the Lomb-Scargle (LS) periodogram (Lomb 1976; Scargle 1982) to determine the most probable period of a variable star. The LS method is useful to estimate periodicities even in the case of unevenly spaced data. We used the

Table 3. The classification of variables.

Prisinzano et al. (2011) class0/I/II sources	Spectral index (α)	Present Classification
V1	-0.715±0.713	MS
V2	—	CTTS
V3	—	CTTS
V4	-0.813±0.132	CTTS
V6	-0.802±0.113	CTTS
V7	-0.963±0.044	CTTS
V8	-0.930±0.096	CTTS
V9	-1.279±0.158	CTTS
V10	-1.471±0.045	CTTS
V13	-0.585±0.030	CTTS
V15	0.490±0.155	CTTS
V16	-0.524±0.220	CTTS
V17	-1.221±0.113	CTTS
V18	-0.690±0.159	CTTS
V19	-1.122±0.170	CTTS
V20	-1.109±0.116	CTTS
V21	-1.576±0.476	CTTS
V22	-0.753±0.369	CTTS
V24	-2.128±0.525	WTTS
V25	-1.297±0.173	CTTS
V26	-1.277±0.089	CTTS
V28	-1.722±0.339	CTTS
V30	-1.089±0.039	CTTS
V32	-1.282±0.114	CTTS
V33	-2.608±0.056	WTTS
V35	-1.131±0.140	CTTS
V39	-2.808±0.111	MS/Herbig Be
V40	-1.837±0.015	WTTS
V43	-1.862±0.516	WTTS
V46	—	Herbig Ae/Be
V52	-2.877±0.046	MS
<hr/>		
diskless sources		
V11	-2.629±0.106	WTTS
V12	-3.035±0.082	MS/Field
V14	-2.741±0.075	WTTS
V23	-2.701±0.130	WTTS
V29	-2.354±0.164	WTTS
V31	-2.575±0.105	WTTS
V34	—	WTTS
V44	-2.209±0.137	WTTS
V47	-2.645±0.089	WTTS
V48	-2.389±0.083	WTTS
V49	—	Herbig Ae/Be
V50	-2.786±0.066	MS
V51	-2.678±0.095	MS
V53	-2.838±0.050	MS/Herbig Be
<hr/>		
not classified by Prisinzano et al. (2011)		
V5	—	YSO/Field
V27	—	YSO/Field
V36	—	MS/Field
V37	—	MS
V38	—	MS
V41	—	MS/Field
V42	—	MS
V45	—	MS

algorithm available at the Starlink³ software database. The periods were further verified with the software period04⁴ (Lenz & Breger 2005). The software period04 provides the frequency and semi-amplitude of the variability in a light curve. Periods derived from the LS method and Period04 generally matched well. The light curves of variable stars are folded with their estimated period. The phased light curves of variable stars identified as CTTSs, WTTSs, probable YSOs and non-YSOs are shown in Figs. 9, 10, 11 and 12, respectively, where averaged differential magnitude in 0.04 phase bin along with σ error bars have been plotted.

Zhang et al. (2008) identified 10 B-type variable stars towards the direction of NGC 1893. Of these, 7 stars (no 6, 8, 10, 3, 5, 9 and 1 in Zhang et al. 2008) are common with our present work (V6, V38, V40, V41, V51, V52 and V53). Three variable stars, namely star nos. 2, 4, 7 of Zhang et al. (2008) were not observed by us.

The star V6 has been classified as a CTTS by Prisinzano et al. (2011) as well as in the present work. Its light curve suggests that it could be an eclipsing binary. Zhang et al. (2008) have reported it an INSA type variable. They derived

two values for the period as 5.747 day and 2.041 day, whereas the values for amplitudes are 0.029 mag and 0.010 mag. Our data suggest a period of 9.68 day and a much larger amplitude, 0.60 mag.

We confirm the variability of V38 suspected by Zhang et al. (2008). Its location in the $V/V - I$ CMD suggests an MS star. Massey et al. 1995 found it to be a B-type star.

Zhang et al. (2008) also found photometric variations in V40 and V41. The present study confirms their variability. The period estimates (0.257, 0.273 and 5.747 day) for V41 by Zhang et al. (2008) do not match with the present period estimate (0.67 day).

Star V51 seems to be a B-type MS star. Marco & Negueruela (2002) also found it to be a B-type star. The variability in star V51 has also been detected by Zhang et al. (2008) and they found a period of 10.0 day. The present work suggests that it could be an irregular type variable (cf. Section 6.1).

Stars V52 and V53 could be MS B-type/Herbig Be stars. Zhang et al. (2008) identified star V53 as B-type variable while in case of V52 they suspected it to be a variable. They estimated the period and amplitude for V53 as 0.26 day and 0.01 mag. In the present work we confirm the variability of V52.

³ <http://www.starlink.uk>

⁴ <http://www.univie.ac.at/tops/Period04>

Table 5. Physical parameters of stars obtained from SEDs.

ID	Disk mass M_{\odot}	σ M_{\odot}	Disk Accretion Rate M_{\odot}/yr	σ M_{\odot}/yr
V1	2.235×10^{-4}	5.018×10^{-4}	8.493×10^{-10}	8.461×10^{-10}
V4	4.390×10^{-3}	1.545×10^{-2}	2.432×10^{-08}	2.542×10^{-08}
V6	8.818×10^{-3}	1.878×10^{-2}	2.395×10^{-08}	2.326×10^{-08}
V7	2.684×10^{-2}	4.083×10^{-2}	6.293×10^{-07}	7.073×10^{-07}
V8	1.738×10^{-2}	2.449×10^{-2}	1.040×10^{-07}	1.015×10^{-07}
V9	7.637×10^{-3}	2.108×10^{-2}	6.864×10^{-08}	6.735×10^{-08}
V10	6.436×10^{-3}	1.346×10^{-2}	3.262×10^{-08}	3.199×10^{-08}
V11	1.075×10^{-2}	1.600×10^{-2}	1.428×10^{-08}	1.406×10^{-08}
V13	2.288×10^{-2}	4.271×10^{-2}	1.807×10^{-07}	1.772×10^{-07}
V14	1.004×10^{-3}	1.150×10^{-3}	2.607×10^{-09}	2.487×10^{-09}
V15	6.723×10^{-3}	1.339×10^{-2}	2.826×10^{-09}	2.754×10^{-09}
V16	1.807×10^{-2}	2.208×10^{-2}	1.469×10^{-07}	1.411×10^{-07}
V17	1.322×10^{-2}	2.050×10^{-2}	4.159×10^{-08}	3.987×10^{-08}
V18	1.404×10^{-2}	1.992×10^{-2}	2.444×10^{-08}	2.383×10^{-08}
V19	4.461×10^{-3}	7.915×10^{-3}	2.188×10^{-08}	2.129×10^{-08}
V20	9.360×10^{-4}	8.594×10^{-4}	3.903×10^{-09}	3.872×10^{-09}
V21	5.105×10^{-3}	1.449×10^{-2}	2.345×10^{-08}	2.449×10^{-08}
V22	1.866×10^{-2}	3.846×10^{-2}	1.438×10^{-07}	1.422×10^{-07}
V23	1.296×10^{-3}	5.484×10^{-3}	3.087×10^{-09}	5.101×10^{-09}
V24	2.251×10^{-3}	9.066×10^{-3}	3.481×10^{-09}	3.565×10^{-09}
V25	2.830×10^{-3}	5.891×10^{-3}	2.855×10^{-09}	2.802×10^{-09}
V26	5.537×10^{-3}	8.124×10^{-3}	1.793×10^{-08}	1.778×10^{-08}
V28	3.943×10^{-3}	1.686×10^{-2}	2.608×10^{-08}	2.770×10^{-08}
V29	1.660×10^{-3}	6.710×10^{-3}	3.390×10^{-09}	3.985×10^{-09}
V30	2.991×10^{-2}	4.062×10^{-2}	2.004×10^{-07}	1.953×10^{-07}
V31	1.289×10^{-3}	5.036×10^{-3}	3.616×10^{-09}	3.839×10^{-09}
V32	2.737×10^{-2}	3.848×10^{-2}	4.517×10^{-07}	4.457×10^{-07}
V33	1.605×10^{-2}	8.095×10^{-3}	5.469×10^{-08}	5.431×10^{-08}
V35	3.600×10^{-2}	2.876×10^{-2}	1.045×10^{-07}	9.988×10^{-08}
V40	1.283×10^{-2}	1.382×10^{-2}	2.203×10^{-09}	2.159×10^{-09}
V43	1.283×10^{-2}	1.382×10^{-2}	1.342×10^{-08}	1.315×10^{-08}
V44	2.916×10^{-3}	9.517×10^{-3}	1.201×10^{-08}	1.652×10^{-08}
V47	6.960×10^{-4}	1.494×10^{-3}	1.613×10^{-09}	1.565×10^{-09}
V48	4.096×10^{-3}	7.598×10^{-3}	3.721×10^{-08}	3.684×10^{-08}

5 PHYSICAL STATE OF VARIABLE STARS

In order to characterize the circumstellar disk properties of YSOs we have analysed the SEDs of the young population associated with the young open cluster NGC 1893. To construct an SED we used multiwavelength i.e optical (V, I), NIR (JHK), mid IR *Spitzer* IRAC (at four wavelengths 3.6, 4.5, 5.8 and 8 micron), NASA’s Wide-field Infrared Survey Explorer (WISE) at 3.4, 4.6, 12, and 22 micron data and fitting tool of Robitaille et al. (2007). Of the 53 detected variables, 45 stars are found in the Prisinzano catalogue. Only 34 stars of 53 variable candidates have their WISE counterparts. Two probable YSOs V5 and V27 were not cross identified in WISE catalogue also, therefore we could not construct the SEDs for these stars. The SED fitting tool of Robitaille et al. (2007) fits thousands of models to the observed SED simultaneously. This SED fitting tool determines their physical parameters like interstellar extinction, temperature, disk mass, disk mass accretion rate, etc. The SED fitting tool needs magnitudes, interstellar extinction A_V and distance of the object as input parameters. The SED fitting tool fits each of the models to the data, allowing both the distance and external foreground extinction to be free parameters. As discussed in Section 3.3 the estimation of $E(B - V)$ for YSOs is not possible on the basis of $U - B/B - V$ TCD, the A_V for each YSO has been estimated using the NIR TCD as follows. The interstellar extinction A_V for a YSO lying in the ‘F’ and ‘T’ region of NIR TCD (cf. Fig. 7) has been obtained by tracing them back to the intrinsic locus of TTSs. In the case of other sources which do not lie in ‘F’ and ‘T’ regions, the A_V of the YSO lying spatially near to the source is applied. Considering the uncertainties that might have gone into the estimation of A_V value of each source, we used the estimated value A_V of each

individual source with a possible range of error as $A_V \pm 2$ mag as input to the model. The distance range is given as 3.0 to 3.6 kpc. The error in NIR and MIR flux estimates due to possible uncertainties in the calibration, extinction, and intrinsic object variability was set as 10%-15%.

The physical parameters like accretion disk mass and accretion rate of probable YSOs constrained from the SED fitting tool are given in Table 5. They have been obtained using the criterion $\chi^2 - \chi_{min}^2 \leq 3N_{data}$ as suggested by Robitaille et al. (2007), where χ_{min}^2 is the goodness of fit parameter for the best fit model and N_{data} is the number of input observational data points. The SED fitting for two variables V10 and V11 is shown in Fig. 13 as examples. The tabulated parameters are obtained from the weighted mean and standard deviation of all the models that satisfy the above mentioned criterion, weighted by the inverse square of the χ^2 of each model. The errors in accretion disk mass and accretion rate given in Table 5 are large because we are dealing with a large parameter space with a limited number of observational data points especially towards longer wavelengths.

6 CHARACTERISTICS OF VARIABLE STARS

6.1 Non-periodic variables

A few stars in our sample seem to show irregular brightness variations. Star V26 seems to have irregular photometric variations (Fig. 9). This star could be irregular variable and its period estimate might be wrong. The light curve of V51 also shows irregular variations (See Fig. 5). On first intra-night observations, its brightness dropped up to ~ 0.1 mag and within one and half hour its luminosity appeared to

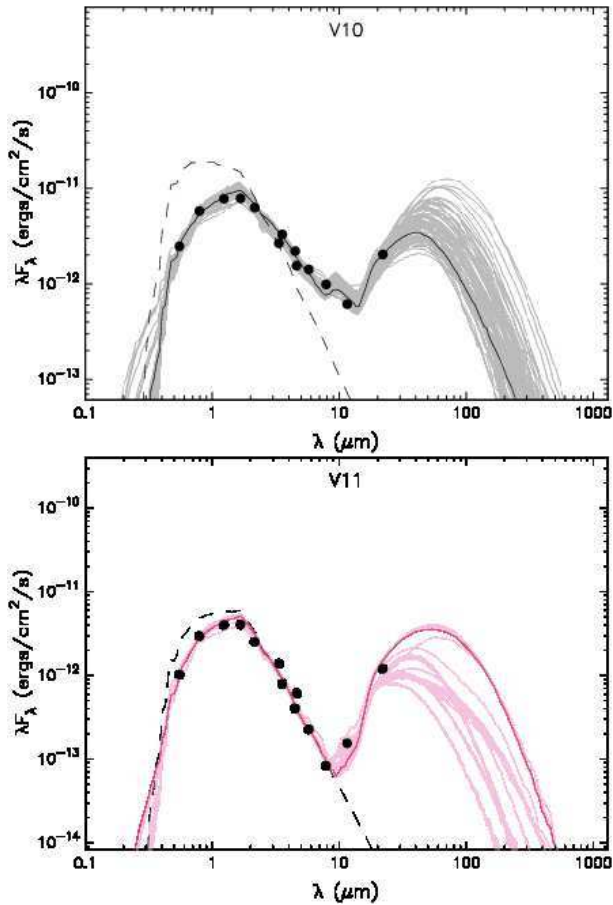


Figure 13. The spectral energy distribution for V10 and V11 PMS stars. The filled circles denote the observed flux. The black line shows the best fit and the grey lines show possible range of good fits. The dashed line shows the stellar photosphere corresponding to the central source of the best-fit model. The results of the best-fit model in each case are given in Table 5.

reach its maximum brightness, while on second intra-night observations it showed no sign of brightness modulation and remained at its maximum brightness. If we consider it to be a short period variable, the first two intra-night observations yield a period of 0.36 day, whereas the last two intra-night observations on 2008 October 29 and 2008 November 21 give a period of 0.61 day. The entire data set for this star suggests a period of 2.86 day. This indicates that star V51 is either pulsating with multiperiod or it might be an eruptive variable. As discussed in Section 4 this star could be a B-type star. Since B-type stars are found to have multiple pulsation periods, it could be multiperiodic B-type star. Its absolute magnitude (0.47 mag) and intrinsic $B - V$ colour (-0.24 mag) put this star in the $H - R$ diagram in the location of γ Cassiopeiae variables, which are irregular variable having outflow of matter. The $(B - V)$ value of star has been taken from WEBDA⁵.

6.2 Periodic variables

The periodic variations in TTSs are believed to occur due to the axial rotation of a star with an inhomogeneous surface, having either hot or cool spots (Herbst et al. 1987, 1994). Herbst et al. (1994) identified three types of day to weeks timescale variability in TTSs. Type I variability, most often seen in WTT variables, is characterized by a smaller stellar flux variations (a few times 0.1 mag) and results from the rotation of a cool spotted photosphere. Type II variables have larger brightness variations (up to 2 mag), most often irregular but sometimes periodic and associated with short-lived accretion related hot spots at the stellar surface of CTT variables. The rare type III variations are characterized by luminosity dips lasting from a few days up to several months, which presumably result from circumstellar dust obscuration.

The majority of the PMS variables detected in the present study have masses $\lesssim 3 M_{\odot}$ and these variables could be TTSs. The estimated periods of these probable TTSs are in the range of 0.15 to 118.09 day, with $\sim 75\%$ having periods ≤ 20 day. The period estimates of CTTs range from 0.36 day to 118.09 day, however majority ($\sim 75\%$) have periods less than 20 day. Two CTTs V13 and V15 are found to have longer periods (68.13 day and 118.09 day, respectively). The spectral energy distributions of V13 and V15 indicate IR excess, and $H\alpha$ emission in the case of V15, suggesting circumstellar disks. Edwards et al. (1993) found that the stars whose $H - K$ colours indicating the presence of circumstellar disks rotate slower than whose $H - K$ colours indicate the absence of an accretion disk. The period estimates for WTTs vary from 0.15 day to 34.73 day.

The amplitude in case of CTTs has a range of 0.07 to 0.99 mag, while amplitude of WTTs varies from 0.02 to 0.35 mag. This indicates that the brightness of CTTs varies with larger amplitude in comparison to WTTs. This result is in agreement with that by Grankin et al. (2007, 2008) and by Lata et al. (2011). The larger amplitude in the case of CTTs could be due to presence of hot spots on the stellar surface produced by accretion mechanism. Hot spots cover a small fraction of the stellar surface but with a high temperature causing larger amplitude of brightness variations (Carpenter et al. 2001). The smaller amplitude in WTTs suggests dissipation of their circumstellar disks or these stars might have cool spots on their surface which are produced due to convection and differential rotation of star and magnetic field.

In the present study we have identified 19 short period variables. The variability characteristics for some of them are discussed individually. The location of V12 on the $U - B/B - V$ TCD and NIR TCD suggests an A-type MS star. It shows persistent variability in its light curve. Its period (0.31 day) is similar to that of W UMa-type eclipsing binary. The shape of the light curve also resembles a W UMa-type variable star, hence it could be A-type W UMa binary star.

The star V14 ($V=15.761$ mag, $mass=2.48 M_{\odot}$) is classified as a WTTs. It shows $H\alpha$ emission. It is a periodic variable with amplitude of 0.16 mag with a period 0.15 day. However its individual night observations on 2008 October 29 and 2010 November 27 give the period of 0.15 and 0.17 day respectively. Its variability characteristics are rather similar to a pulsating PMS star. Its absolute magnitude

⁵ <http://www.univie.ac.at/webda/>

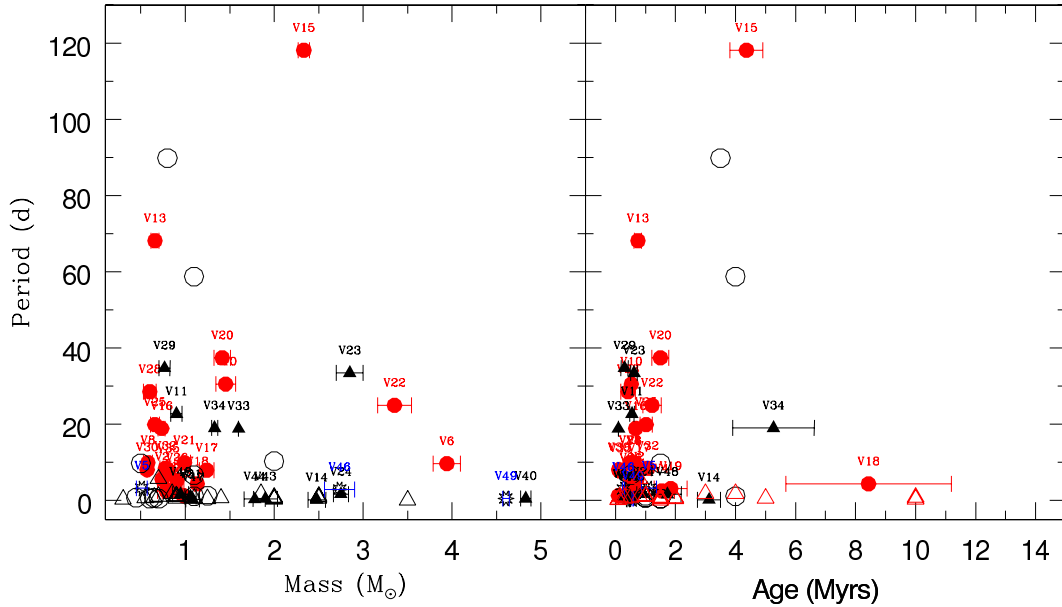


Figure 14. Rotation period of TTSs as a function of mass and age. The symbols are same as in Fig. 8. Starred circles represent probable YSOs. One probable YSO V27 ($P=220.93$) is not plotted in the figure. Open circles and triangles represent data for Be 59 taken from Lata et. al. (2011).

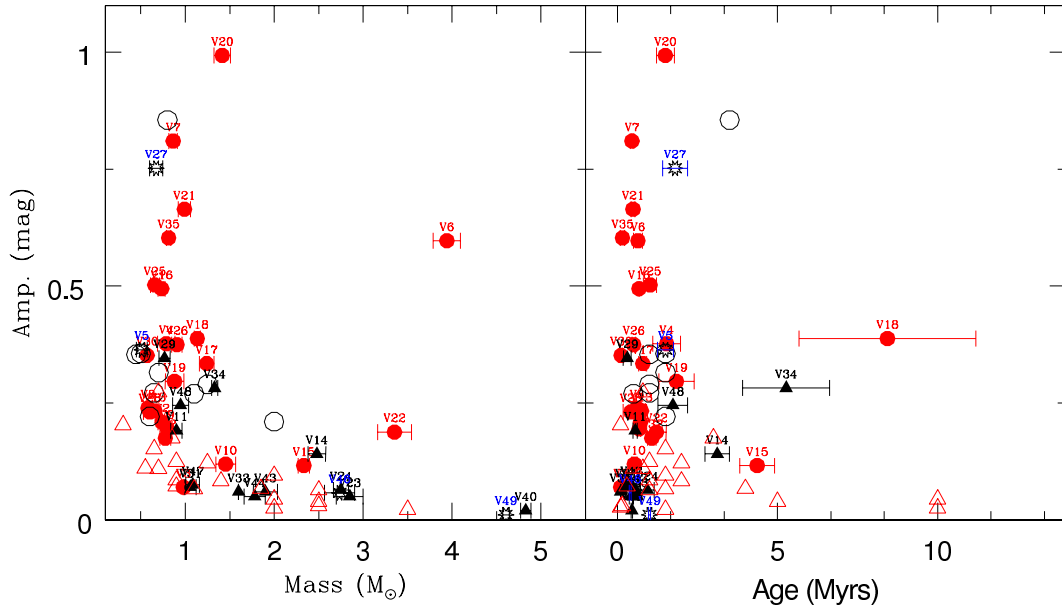


Figure 15. Amplitude of TTSs as a function of mass and age. The symbols are same as in Fig. 8 and Fig. 14. Open circles and triangles represent data for Be 59 taken from Lata. et. al. (2011).

and intrinsic ($B - V$) colour put it on the pulsation strip in the $H - R$ diagram where δ Scuti stars are expected to be located. We feel that star V14 could be a PMS δ Scuti type star. Several previous studies (e.g. Breger 1972; Kurtz & Marang 1995; Marconi et al. 2000; Donati et al. 1997; Zwintz et al. 2005, 2009; Zwintz & Weiss 2006) have already reported PMS pulsators ($\gtrsim 2M_{\odot}$) in the instability region as they evolve to the MS. A combination of mass, temperature and luminosity of these stars make them to pulsate (Zwintz et al. 2005, 2009).

The light curve of V36 indicates an eclipsing binary. It

is a relatively faint star ($V=17.958$ mag) located at ~ 6.0 arcmin away from the cluster centre. Stars V37 and V38 are found to be located on the MS in the $V/V - I$ CMD. Star V38 is a confirmed B-type MS star with an emission-line spectrum (Zhang et al. 2008), whereas V37 could also be a B-type MS star according to Marco & Negueruela (2002). Their variability characteristics like amplitude, period and shape of the light curve also suggest B-type pulsating stars.

The locations of stars V39, V40, V42, V45, V49, V52 and V53 in the $V/V - I$ CMD (Fig. 8) indicate that these stars have masses $\gtrsim 3 M_{\odot}$. Marco & Negueruela (2002) have

classified V40 as a Herbig Be star with a spectral type B0.5 IVe. The light curves of V39, V40 and V42 are rather similar, with periods 0.32 day, 0.48 day and 0.31 day and amplitudes 0.02, 0.20 and 0.02 mag, respectively. The light curves of V49 shows a different behaviour from these three stars. The location of V39 and V49 in the $J-H/H-K$ TCD lies in the region of Herbig Ae/Be stars. The location of V39, V40 and V49 in $U-B/B-V$ TCD suggests that these star probably have excess in the U -band. We classify V39, V40, V42 and V49 as Herbig Be type stars. The variability characteristics of V45, V52 and V53 show that these stars could be B-type stars.

The period and shape of the light curve of star V41 (period=0.67 day and amp=0.04 mag) indicate that it could be a pulsating star similar to an RR Lyrae variable. RR Lyrae variables are similar to Cepheids, but less luminous and have periods of 0.5 to 1 day. Its spectral type F0 III-IV (Marco & Negueruela 2002) also suggests an RR Lyrae type variable. The above discussion indicates that this star could not be young enough to be a part of the cluster NGC 1893.

The location of V50 on the $J-H/H-K$, $U-B/B-V$ CC diagram and $V, V-I$ CMD indicates that it could be a MS B-type star. The shape of the light curve and variability characteristics (period=0.58 day and amp=0.02 mag) put it in a category of B-type pulsating stars. Its absolute magnitude and intrinsic ($B-V$) colour lie in the region of β Cep variable stars in the $H-R$ diagram. Its light curve is also similar to that of β Cephei type variable stars. The β Cephei type variable stars have periodical pulsations in the range of 0.1 to 0.6 day with an amplitude of 0.01 to 0.3 mag.

To understand the correlation of mass and age of the TTSs on the rotation period we plot the rotation period as a function of mass and age in Fig. 14. To increase the sample we have also included data for Be 59 from Lata et al. (2011) because this cluster has similar environment to the NGC 1893, and moreover the same technique has been used to identify variable stars and determine their physical properties. Although there is a large scatter, the stars having masses $\gtrsim 2M_{\odot}$ are found to be fast rotators. Similarly, the stars having ages $\gtrsim 3$ Myr seem to be fast rotators. This result is compatible with the disc locking model in which it is expected that the population of stars with disc rotate slowly than those without disc (Edwards et al. 1993; Herbst et al. 2000; Littlefair et al. 2005). In a recent study Littlefair et al. (2011) pointed out “if the location of a star in the CMD is interpreted as being due to genuine age spreads within a cluster, then the implication is that the youngest stars in the cluster (those with the largest moments of inertia and highest likelihood of ongoing accretion) are the most rapidly rotating. Such a result is in conflict with the existing picture of angular momentum evolution in young stars, where the stars are braked effectively by their accretion discs until the disc disperses”. Alternatively, they argued that the location of the stars in the CMD is not primarily a function of age, but of accretion history. They discussed that this hypothesis can, in principle, explain the observed correlation between rotation rate and location of the star in the CMD. It is worthwhile to point out that the study by Littlefair et al. (2011) assumes that the stars in the mass range $0.4 \leq M/M_{\odot} < 1$ have little dependence between rotation rate and stellar mas. However, in the present

study we find that relatively massive stars in the mass range $0.5 \leq M/M_{\odot} < 1.3$ have faster rotation.

Fig. 15 reveals that amplitude of TTSs variability is correlated with the mass (left panel) and age (right panel) in the sense that amplitude decreases with increase in mass as well as age of variable star. The star V6 does not seem to follow the mass-amplitude trend. This star has a large IR excess and shows a large variation in the amplitude (0.10 and 0.29 mag; Zhang et al. 2008.; 0.60 mag; present work). It could be either a star whose brightness variation is supposed to be produced by obscuration due to dust clumps or clouds as in the case of Type III variability characteristics suggested by Herbst et al. (1994) or it might be an eclipsing binary. The stars V18 (Class II source) and V34 (Class III source) have ages > 5 Myr and do not follow the general decreasing trend in amplitude-age distribution (Fig. 15, right panel). The star V18 is undoubtedly a Class II source as it shows NIR excess. Its amplitude is ~ 0.40 mag. If its V magnitude given in Table 2 is at minimum, its age will be overestimated on the basis of $V/V-I$ CMD. Similarly the star V34 has amplitude ~ 0.3 mag. Its mean V magnitude could yield an age of ~ 3 Myr. Baraffe et al. (2009) have shown that the higher age of young low mass stars could be results of episodic accretion which produces a luminosity spread in the HR diagram at ages of a few Myr.

The decrease in amplitude could be due to the dispersal of the disk. This result further supports the notion, as obtained in our previous study of Be 59 (Lata et al. 2011) that the disk dispersal mechanism is less efficient for relatively low mass stars. Fig. 15 (right panel) manifests that significant amount of the disks is dispersed by $\lesssim 5$ Myr. This result is in accordance with the result obtained by Haisch et al. (2001).

Fig. 16 plots amplitude as a function of disk mass and disk accretion rate. We did not find any correlation between amplitude and disk mass as well as disk accretion rate.

7 SUMMARY

The paper presents time series photometry of 53 variable stars identified in the cluster NGC 1893 region. The probable members associated with the cluster are identified on the basis of spectral energy distribution, location in the $V/V-I$ CMD and $J-H/H-K$ TCD. Forty three variables are found to be probable PMS stars. The majority of these sources have ages $\lesssim 5$ Myr and masses in the range of $0.5 \lesssim M/M_{\odot} \lesssim 4$ and hence should be TTSs. The rotation periods of majority of TTSs ranges from 0.1 to 20 day. The brightness of CTTSs varies with larger amplitude in comparison to that of WTTSs. Both the period and amplitude of variability of TTSs decrease with increasing mass. This confirms our earlier finding that decrease in amplitude of variability in relatively massive stars could be due to the dispersal of circumstellar disk. This result supports our earlier result (Lata et al. 2011) that mechanism of disk dispersal operates less efficiently for relatively low mass stars.

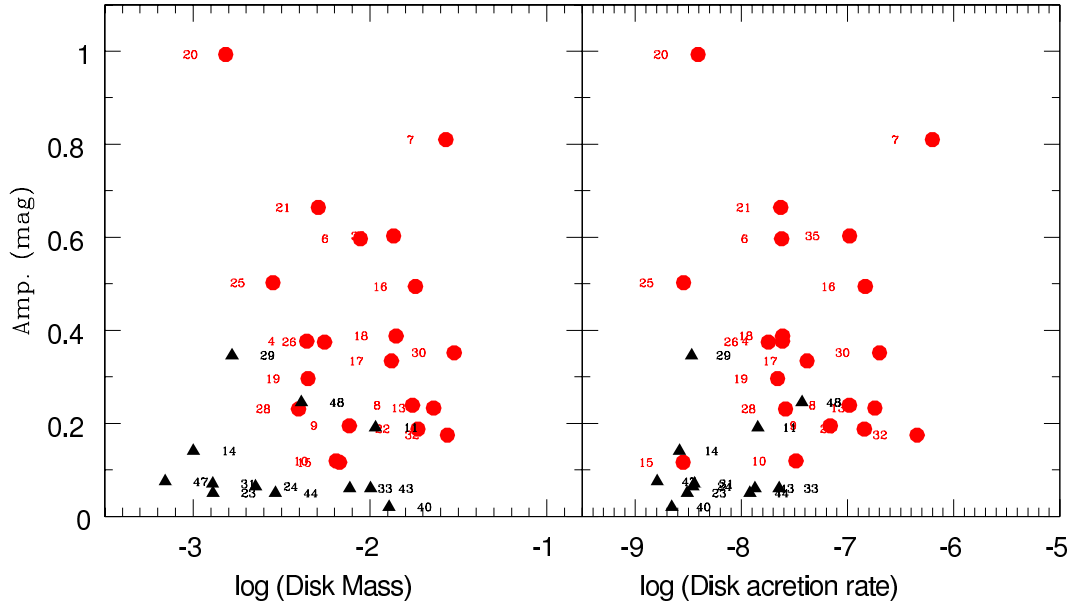


Figure 16. Amplitude of TTSs as a function of disk mass and disk mass accretion rate. The symbols are same as in Fig. 8.

8 ACKNOWLEDGMENTS

Authors are very thankful to the anonymous referee for a critical reading of the paper and useful scientific suggestions that improved scientific content of the paper. Part of this work was carried out by AKP during his visit to National Central University (Taiwan) under India-Taiwan collaborative program. AKP is thankful to the GITA, DST (India) and NSC (Taiwan) for the financial help.

REFERENCES

- [Appenzeller I., & Mundt R., 1989, *Astron. Astrophys. Rev.* 1, 291
- [Baraffe I., Chabrier G., Gallardo J., 2009, *ApJ*, 702L, 27
- [Bouvier J., 1994, in *Astronomical Society of the Pacific Conference Series*, Vol. 64, *Cool Stars, Stellar Systems, and the Sun*, J.-P. Caillault, ed., pp. 151
- [Bouvier J., Cabrit S., Fernandez M., Martin E. L., Matthews J. M., 1993, *A&AS*, 101, 485
- [Breger M., 1972, *ApJ*, 176, 367
- [Bessell M. S., Brett J. M., 1988, *PASP*, 100, 1134
- [Chauhan N., Pandey A. K., Ogura K., Ojha D. K., Bhatt B. C., Ghosh S. K., Rawat P. S., 2009, *MNRAS*, 396, 964
- [Chauhan N., Pandey A. K., Ogura K., Jose J., Ojha D. K., Samal M. R., Mito H., 2011, *MNRAS*, 415, 1202
- [Carpenter J. M., Hillenbrand L. A., Skrutskie M. F., 2001, *AJ*, 121, 3160
- [Cutri R. M., Skrutskie M. F., van Dyk S., et al., 2003, *2MASS All Sky Catalog of point sources*.
- [Cohen J. G., Persson S. E., Elias J. H., Frogel J. A., 1981, *ApJ*, 249, 481
- [Donati J. -F., Semel M., Carter B. D., Rees D. E., Collier Cameron A., 1997, *MNRAS*, 291, 658
- [Edwards S., Strom S. E., Hartigan P., Strom K. M., Hillenbrand L. A., Herbst W., Attridge J., Merrill K. M., Probst R., Gatley I., 1993, *AJ*, 106, 372
- [Girardi L., Bertelli G., Bressan A., Chiosi C., Groenewegen M. A. T., Marigo P., Salasnich B., & Weiss A., 2002, *A&A*, 391, 195
- [Gaze V. F., Shajn G. A., 1955, *Izvestiya Ordena Trudovogo Krasnogo Znameni Krymskoj Astrofizicheskoj Observatorii*, 15, 11
- [Grankin K. N., Melnikov S. Yu., Bouvier J., Herbst W., Shevchenko V. S., 2007, *A&A*, 461, 183
- [Grankin K. N., Bouvier J., Herbst W., Melnikov S. Y., 2008, *A&A*, 479, 827
- [Haisch K. E., Lada E. A., Lada C. J. 2001, *ApJ*, 553, L153
- [Herbst W., Booth J. F., Korett F. L., et al, 1987, *AJ*, 94, 137
- [Herbst W., Herbst D. K., Grossman E. J., Weinstein D., 1994, *AJ*, 108, 1906
- [Herbst W., Maley J. A., Williams E. C., 2000, *AJ*, 120, 349
- [Hillenbrand L. A, 2002, *astro.ph.10520*
- [Hiltner W. A., 1966, in *IAU Symposium*, Vol. 24, *Spectral Classification and Multicolour Photometry*, K. Loden, L. O. Loden, & U. Sinnerstad, ed., pp. 373–+
- [Kurtz D. W., Marang F., 1995, *MNRAS*, 276, 191
- [Lada C. J., Muench A. A., Luhman K. L., et al., 2006, *AJ*, 131, 1574
- [Lata S., Pandey A. K., Maheswar G., Mondal S., Kumar B., 2011, *MNRAS*, 418, 1346
- [Lenz P., Breger, M. *Comm. Asteroseismol.*, 146,53
- [Littlefair S. P., Naylor T., Burningham B., Jeffries R. D., 2005, *MNRAS*, 358, 341
- [Littlefair S. P., Naylor T., Mayne N. J., Saunders E., Jeffries R. D., 2011, *MNRAS*, 413, 56
- [Lomb N.R., 1976, *ApSS*, 39, 447
- [Landolt A. U., 1992, *AJ*, 104, 340
- [Maheswar G., Sharma S., Biman J. M., Pandey A. K., Bhatt H. C., 2007, *MNRAS*, 379, 1237

- Marco A., Bernabeu G., Negueruela I., 2001, *AJ*, 121, 2075
- Marco A., Negueruela I., 2002, *A&A*, 393, 195
- assey P., Johnson K. E., Degioia-Eastwood K., 1995, *ApJ*, 454, 151
- Marconi M., Ripepi V., Alcalá J. M., Covino E., Palla F., Terranegra L., 2000, *A&A*, 355, L35
- Meyer M. R., Calvet N., Hillenbrand, L. A., 1997, *AJ*, 114, 288
- Negueruela I., Marco A., Israel G. L., Bernabeu G., 2007, *A&A*, 471, 485
- Percy J. R., Gryc W. K., Wong J., Herbst W., 2006, *PASP*, 118, 1390
- Percy J. R., Grynko S., Seneviratne R., Herbst W., 2010, *PASP*, 122, 753
- Prisinzano L., Sanz-Forcada J., Micela G., Caramazza M., Guarcello M. G., Sciortino S., Testi L., 2011, *A&A*, 527, 77
- Robitaille T. P., Whitney B. A., Indebetouw R., Wood K., 2007, *ApJS*, 169, 328
- Scargle J.D., 1982, *ApJ*, 263, 835
- Siess L., Dufour E., Forestini M., 2000, *A&A*, 358, 593
- Schaefer B. E., 1983, *ApJ*, 266, L45
- Sharma S., Pandey A. K., Ojha D. K., Chen W. P., Ghosh S. K., Bhatt B. C., Maheswar G., Sagar R., 2007, *MNRAS*, 380, 1141
- Stetson P. B., 1987, *PASP*, 99, 191
- Stetson P. B., 1992, *J. R. Astron. Soc. Can.*, 86, 71
- Vallenari A., Richichi A., Carraro G., Girardi L., 1999, *A&A*, 349, 825
- Zhang C., Fu J. N., Jiang X. J., 2008, *JPhCS*, 118, 2078
- Zwintz K., Marconi M., Reegen P., et al. 2005, *MNRAS*, 357, 345
- Zwintz K., Weiss W. W., 2006, *A&A*, 457, 237
- Zwintz K., Hareter M., Kuschnig R., et al., 2009, *A&A*, 502, 239